Flow of a Burgers fluid due to time varying loads on deforming boundaries

J. Hron[a], K. R. Rajagopal[b], K. Tůma[a,b,*]

[a] *Charles University in Prague, Faculty of Mathematics and Physics, Mathematical Institute of Charles University, Sokolovská 83, 186 75 Prague 8, Czech Republic*
[b] *Department of Mechanical Engineering, Texas A&M University, College Station, TX 77843, USA*

Abstract

In this paper we study three boundary-initial value problems within the context of four rate type viscoelastic constitutive models, the Maxwell model, the Oldroyd-B model, Burgers model and the generalized Burgers model. We consider challenging problems wherein the boundary is deforming with time. The flows lead to complex system of partial differential equations that require the development of a robust numerical procedure based on the arbitrary Lagrangian-Eulerian method. In addition to providing very valuable information concerning the unsteady response of popular viscoelastic fluid models in complex loading conditions, these boundary value problems have relevance to important technological problems concerning the unsteady response of asphalt concrete pavements due to a variety of loading conditions.

Keywords: Rate type fluid, Maxwell, Oldroyd-B, Burgers, finite element method, monolithic ALE method.

1. Introduction

The response of many viscoelastic fluids can be captured reasonably well by rate type fluid models. The earliest and the most popular rate type fluid model is that due to Maxwell [1] who developed a one dimensional model. Later, Burgers [2] developed a one dimensional rate type fluid model which includes the Maxwell model as a special case. A proper framework to develop frame indifferent three dimensional models was put into place by Oldroyd [3] and amongst the several models that he proposed one that has become very popular is the Oldroyd-B model. Burgers' one dimensional model includes the one dimensional Oldroyd-B model as a special case. These rate type models have been used to describe the behavior of a wide spectrum of materials: dilute polymeric fluids, asphalt and asphalt concrete, biological fluids, volcanic lava, glaciers, etc.

*Corresponding author.
Email addresses: hron@karlin.mff.cuni.cz (J. Hron), krajagopal@tamu.edu (K. R. Rajagopal), ktjunior@seznam.cz (K. Tůma)

In view of their usefulness in describing the response of a wide variety of materials, many boundary-initial value problems have been solved within the context of these fluids. Usually the Maxwell and Oldroyd-B models are used in the simulations and we mention a few of them. For example, in a recent study, Damanik [4] in his Ph.D. thesis simulated the flows of Oldroyd-B and Giesekus model in a fixed domain in an Eulerian framework with FEM, he dealt with flows at high Weissenberg number wherein one encounters numerical difficulties that is referred to as the "High Weissenberg number Problem" (for more details about this problem see White et al. [5]) which can be solved using LCR reformulation introduced by Fattal and Kupferman [6]. One of the problems he solved was the benchmark problem of a planar flow of Oldroyd-B model around the cylinder where the drag force is computed, this problem has been studied numerically in many papers using both the finite element method and the finite volume method (see for example Hulsen et al. [7], Afonso et al. [8], Fan et al. [9] or the paper by Damanik et al. [10]).

The problem of free-surface flow was studied by Étienne et al. [11]; they studied the collapse of a column of Oldroyd-B fluid with the help of arbitrary Lagrangian-Eulerian formulation for low/moderate Weissenberg numbers. Alternative approach for free surface problem is used in Damanik et al. [12] where the level set method is used for interface tracking between the viscoelastic bubble and the surrounding fluid. This approach has the capability to capture topological changes of the interface. We are also interested in problems involving free and deforming surfaces and the applications we have in mind are problems involving the flow of asphalt and asphalt concrete where one does not expect topological changes of the interface. In general these materials have been notoriously difficult to model (see the review article of Krishnan and Rajagopal [13] for a discussion of the relevant issues) and the popular model of choice for such materials is the model due to Burgers [2]. For the applications that we have in mind such as the compaction of asphalt layers, etc., the flow takes place at low to moderate Weissenberg numbers and hence we shall study such flows. Our study is not just relevant to the flow of asphalt. The most popular model for describing the earth's mantle is also the Burgers fluid model, and as the model includes the Oldroyd-B and Maxwell models as special sub-classes our study is relevant to a very large class of problems wherein the boundary is undergoing time-dependent deformations. We solve problems with a deforming free surface by transforming the equations from Eulerian description into arbitrary Langrangian-Eulerian description. The way how the equations are transformed is universal and can be easily used for implementing every viscoelastic rate type fluid model, even non-linear models. We are mainly interested in simulating Burgers' model which has not been so far simulated when free surface is deforming and which is capable of describing the response of material with more than one relaxation mechanism.

The problems with the viscoelastic fluid model under consideration is quite complicated and intricate as the constitutive relation is given by an implicit equation that relates the stress and properly invariant time derivatives of the stress and the symmetric part of the velocity gradient and its properly invariant time derivatives. Thus, unlike the classical theories of fluids such as the Euler fluid or the Navier-Stokes fluid, or constitutive theories wherein one has an explicit expression for the stress in terms of kinematical variable, which will allow us to substitute the expression for the same in the balance of linear momentum to obtain a partial differential equation for the velocity field, we will have to solve the system of equations comprising the constitutive equations and the basic balance laws simultaneously. The equations governing the flow of such fluids in general three dimensional problems in

finite domains are most challenging and in this paper we consider three such problems that have relevance to interesting real world applications.

We consider three typical boundary-initial value problems. The first problem that we consider is a block of viscoelastic material that is initially at rest being subject to a compressive load on a part of the top surface of the block at time $t = 0$, and the compressive load is removed after application for a certain time (see Figure 3). The bottom surface of the block is allowed to slip but not move in the vertical direction, all the other boundaries being allowed to move freely. We then study the evolution of the deformation of the slab with time. The second problem concerns a generalization of the first wherein we consider repeated application of compressive loads at two different locations on the top surface of the slab. In the last problem, we consider a load that is moving on the top surface.

All the problems that we consider have relevance to deformations of a body of asphalt concrete subject to typical loads under field conditions. The first problem would correspond to a static load such as a parked vehicle, while the second problem would correspond to the important technological problem of rutting of roadways, wherein a depression is observed in a portion of the roadways due to the repeated motion of vehicles. The last problem also has relevance to the motion of vehicles over roadways wherein now we just look at the response of a slab to a moving load, the portion of the slab behind the vehicle relaxing towards its natural state.

The organization of the paper is as follows. In the next section, we introduce the Burgers model and a generalization of it. These models contain as special sub-classes two rate type models that are capable of describing the response of viscoelastic fluids: the Maxwell model and the Oldroyd-B model, and generalizations of the same. In Section 3 we discuss the numerical procedure, see for example the book by Crochet et al. [14] for relevant background. After a brief discussion of the unsuitability of the Lagrangian method to study the problem, we discuss the Arbitrary Lagrangian-Eulerian method that is used to simulate the three boundary-initial value problems discussed above. In the final section, we discuss the solution to three boundary-initial value problems.

2. Some standard incompressible viscoelastic rate type fluid models

In this section we introduce the incompressible viscoelastic rate-type fluid models that are used in the simulations due to time varying loads on the boundary..

2.1. Balance laws

We record the balance of mass

$$\frac{\partial \rho}{\partial t} + \mathbf{v} \cdot \nabla \rho + \rho \operatorname{div} \mathbf{v} = 0 \tag{1}$$

and the balance of linear momentum

$$\rho \left(\frac{\partial \mathbf{v}}{\partial t} + \mathbf{v} \cdot \nabla \mathbf{v} \right) = \operatorname{div} \mathbf{T} \,, \tag{2}$$

where $\mathbf{v}$ is the fluid velocity, ρ is the density and $\mathbf{T}$ is Cauchy stress tensor which is symmetric due to the balance of angular momentum in the absence of internal body couples. Since we will be considering incompressible fluids, they can only undergo isochoric motions and hence

$$\operatorname{div} \mathbf{v} = 0. \tag{3}$$

2.2. Maxwell model

Maxwell [1] derived the earliest one dimensional fluid model which when appropriately generalized to three dimensions, in the case of an incompressible fluid, takes the form:

$$\mathbf{T} = -p\mathbf{I} + \mathbf{S}\,, \tag{4}$$

$$\mathbf{S} + \tau \overset{\triangledown}{\mathbf{S}} = 2\eta_e \mathbf{D}\,, \tag{5}$$

where $\mathbf{T}$ is the Cauchy stress, τ is relaxation time and η_e is the viscosity and $-p\mathbf{I}$ is the indeterminate reaction stress due to the constraint of incompressibility, $^{\triangledown}$ is the upper convected Oldroyd derivative defined through

$$\overset{\triangledown}{\mathbf{S}} = \frac{\partial \mathbf{S}}{\partial t} + \mathbf{v}\cdot\nabla\mathbf{S} - (\nabla\mathbf{v})\mathbf{S} - \mathbf{S}(\nabla\mathbf{v})^{\mathrm{T}}. \tag{6}$$

The Maxwell model can be expressed in an alternate manner (see Rajagopal and Srinivasa [15]) using a new tensor $\mathbf{B} = \frac{1}{G}(\mathbf{I} + \mathbf{S})$ in other way that is used in the simulation

$$\mathbf{T} = -p\mathbf{I} + G(\mathbf{B} - \mathbf{I})\,, \tag{7a}$$

$$\overset{\triangledown}{\mathbf{B}} = \frac{1}{\tau}(\mathbf{I} - \mathbf{B})\,, \tag{7b}$$

here instead of viscosity η_e we have introduced elastic modulus G.

2.3. Oldroyd-B model

Oldroyd [3] was the first to systematically derive three dimensional rate type models that satisfied frame-indifference and other invariance requirements. Amongst the several models that he developed, one that is quite popular amongst rheologists is the Oldroyd-B model, which is defined through:

$$\mathbf{T} = -p\mathbf{I} + 2\eta_s\mathbf{D} + \mathbf{S}\,, \tag{8a}$$

$$\mathbf{S} + \tau \overset{\triangledown}{\mathbf{S}} = 2\eta_e \mathbf{D}\,. \tag{8b}$$

The Oldroyd-B model can be expressed in an alternate manner as in case of the Maxwell model (see Rajagopal and Srinivasa [15])

$$\mathbf{T} = -p\mathbf{I} + 2\eta_s\mathbf{D} + G(\mathbf{B} - \mathbf{I})\,, \tag{9a}$$

$$\overset{\triangledown}{\mathbf{B}} = \frac{1}{\tau}(\mathbf{I} - \mathbf{B})\,. \tag{9b}$$

2.4. Burgers model

Before Oldroyd, Burgers [2] had developed a one dimensional rate type constitutive relation which when properly generalized to three dimensions can be expressed as

$$\mathbf{T} = -p\mathbf{I} + \mathbf{S} \tag{10a}$$

$$\mathbf{S} + \lambda_1 \overset{\triangledown}{\mathbf{S}} + \lambda_2 \overset{\triangledown\triangledown}{\mathbf{S}} = \eta_1\mathbf{D} + \eta_2 \overset{\triangledown}{\mathbf{D}}, \tag{10b}$$

where $\lambda_1, \lambda_2, \eta_1$ and η_2 are material parameters. This model includes both the Maxwell models and the Oldroyd-B models as special sub-classes. The three dimensional Burgers model can be expressed in the equivalent form (see Krishnan and Rajagopal [13]):

$$\mathbf{T} = -p\mathbf{I} + G_1(\mathbf{B}_1 - \mathbf{I}) + G_2(\mathbf{B}_2 - \mathbf{I})\,, \tag{11a}$$

$$\overset{\triangledown}{\mathbf{B}}_1 = \frac{1}{\tau_1}(\mathbf{I} - \mathbf{B}_1)\,, \tag{11b}$$

$$\overset{\triangledown}{\mathbf{B}}_2 = \frac{1}{\tau_2}(\mathbf{I} - \mathbf{B}_2)\,, \tag{11c}$$

where G_1, G_2 are elastic moduli and τ_1, τ_2 are relaxation times and so this model is capable of capturing two different relaxation mechanisms (compared to Maxwell or Oldroyd that are capable of capturing only one).We now proceed to show that (10) and (11) are equivalent. First, let us define

$$\mathbf{S}_1 = G_1(\mathbf{B}_1 - \mathbf{I}), \quad \mathbf{S}_2 = G_2(\mathbf{B}_2 - \mathbf{I}), \quad \mathbf{S} = \mathbf{S}_1 + \mathbf{S}_2.$$

Then (11) reduces to

$$\mathbf{T} = -p\mathbf{I} + \mathbf{S}\,, \tag{12a}$$

$$\overset{\triangledown}{\mathbf{S}}_1 = -\frac{1}{\tau_1}\mathbf{S}_1 + 2G_1\mathbf{D}\,, \tag{12b}$$

$$\overset{\triangledown}{\mathbf{S}}_2 = -\frac{1}{\tau_2}\mathbf{S}_2 + 2G_2\mathbf{D}\,. \tag{12c}$$

Using (12b) and (12c) repeatedly we calculate $\overset{\triangledown}{\mathbf{S}}$ and $\overset{\triangledown\triangledown}{\mathbf{S}}$. We obtain

$$\begin{aligned}\overset{\triangledown}{\mathbf{S}} &= \overset{\triangledown}{\mathbf{S}}_1 + \overset{\triangledown}{\mathbf{S}}_2 \\ &= -\frac{1}{\tau_1}\mathbf{S}_1 - \frac{1}{\tau_2}\mathbf{S}_2 + 2(G_1 + G_2)\mathbf{D}\,, \end{aligned} \tag{13}$$

$$\begin{aligned}\overset{\triangledown\triangledown}{\mathbf{S}} &= -\frac{1}{\tau_1}\overset{\triangledown}{\mathbf{S}}_1 - \frac{1}{\tau_2}\overset{\triangledown}{\mathbf{S}}_2 + 2(G_1 + G_2)\overset{\triangledown}{\mathbf{D}} \\ &= \frac{1}{\tau_1^2}\mathbf{S}_1 + \frac{1}{\tau_2^2}\mathbf{S}_2 - 2\left(\frac{G_1}{\tau_1} + \frac{G_2}{\tau_2}\right)\mathbf{D} + 2(G_1 + G_2)\overset{\triangledown}{\mathbf{D}}\,. \end{aligned} \tag{14}$$

Adding $(\tau_1 + \tau_2)\overset{\triangledown}{\mathbf{S}} + \tau_1\tau_2\overset{\triangledown\triangledown}{\mathbf{S}}$ we obtain standard Burgers' models (11)

$$\mathbf{S} + (\tau_1 + \tau_2)\overset{\triangledown}{\mathbf{S}} + \tau_1\tau_2\overset{\triangledown\triangledown}{\mathbf{S}} = 2(\tau_1 G_1 + \tau_2 G_2)\mathbf{D} + 2\tau_1\tau_2(G_1 + G_2)\overset{\triangledown}{\mathbf{D}}\,. \tag{15}$$

2.5. A modified Burgers model with additional Newtonian dissipation

We will use also the Burgers model with additional Newtonian dissipation

$$\mathbf{T} = -p\mathbf{I} + 2\eta_s\mathbf{D} + G_1(\mathbf{B}_1 - \mathbf{I}) + G_2(\mathbf{B}_2 - \mathbf{I})\,, \tag{16a}$$

$$\overset{\triangledown}{\mathbf{B}}_1 = \frac{1}{\tau_1}(\mathbf{I} - \mathbf{B}_1)\,, \tag{16b}$$

$$\overset{\triangledown}{\mathbf{B}}_2 = \frac{1}{\tau_2}(\mathbf{I} - \mathbf{B}_2)\,. \tag{16c}$$

One notices that Oldroyd-B model (9) reduces to a Maxwell model (7) when $\eta_s = 0$ Pa s, the same holds for the generalized Burgers model (16) and Burgers model (11). Further, Burgers (11) reduces to Maxwell model (7) if $\tau_1 = \tau_2 = \tau$ and $G = G_1 + G_2$ if we have the same boundary and initial conditions for $\mathbf{B}_1$ and $\mathbf{B}_2$. Again the same holds for generalized Burgers model (16) and Oldroyd-B model (9). Hence, all models are a special variant of the generalized Burgers model (16). In the next section we show the reformulation to arbitrary Lagrangian-Eulerian description for the generalized Burgers model (16).

2.6. Properties of Burgers model with additional Newtonian dissipation and the apriori estimates

In this subsection we disscuss some of the properties of the generalized Burgers model (16). In order to do so, we adopt a procedure that is similar to that of Boyaval et al. [16]. Initially, being at rest $\mathbf{B}_i(t=0) = \mathbf{I}, i = 1, 2$ are symmetric positive definite matrices with $\det \mathbf{B}_i(t=0) = 1$. We show that they are positive definite for all $t \geq 0$.

From the continuity of $\det \mathbf{B}_i$ and eigenvalues with respect to time t we know that $\det \mathbf{B}_i(t) > 0$ at least upto some certain time t_0, the symmetry is satisfied for all t because (16b) and (16c) are symmetric. Let us suppose that there are times t_0^i such that $\det \mathbf{B}_i(t) > 0, t < t_0^i$ and there is at least one eigenvalue converging to zero for $t \to t_0$, and $\det \mathbf{B}_i(t = t_0^i) \leq 0$. Then for $t < t_0^i$ the matrices $\mathbf{B}_i$ are symmetric positive definite, and the same holds for its inverse. The following inequality that comes from the inequality of arithmetic and geometric mean is used

$$\operatorname{tr} \mathbf{B}_i^{-1} \geq d(\det \left(\mathbf{B}_i^{-1}\right))^{1/d}, \tag{17}$$

where d is the dimension of the space. Now we use equations (16b) and (16c) and compute the material time derivative of $\det \mathbf{B}_i$

$$\begin{aligned}\frac{\mathrm{d}}{\mathrm{d}t}\left((\det \mathbf{B}_i)^{1/d}\right) &= \frac{1}{d}(\det \mathbf{B}_i)^{1/d}\frac{\mathrm{d}}{\mathrm{d}t}(\ln \det \mathbf{B}_i) = \frac{1}{d}(\det \mathbf{B}_i)^{1/d} \operatorname{tr}\left(\dot{\mathbf{B}}_i \mathbf{B}_i^{-1}\right) \\ &\overset{(16b),(16c)}{=} \frac{1}{d}(\det \mathbf{B}_i)^{1/d}\frac{1}{\tau_i}\operatorname{tr}\left(\mathbf{B}_i^{-1} - \mathbf{I}\right) \overset{(17)}{\geq} \frac{1}{\tau_i}\left(1 - (\det \mathbf{B}_i)^{1/d}\right).\end{aligned}$$

If we denote $x_i := (\det \mathbf{B}_i)^{1/d}$ we obtain an ODE for x_i, with $x_i(0) = 1$

$$\tau \dot{x}_i + x_i \geq 1 \Leftrightarrow \tau_i \dot{x}_i + x_i = K_i(t) \geq 1, \quad i = 1, 2.$$

The solutions of these two ordinary differential equations are

$$x_i(t) = \left(1 + \frac{1}{\tau_i}\int_0^t K_i(s) e^{s/\tau}\,\mathrm{d}s\right) e^{-t/\tau_i}, 0 \leq t < t_0^i$$

greater or equal than one for $t < t_0^i$. From the continuity of $\det \mathbf{B}_i$ w.r.t. time t we also have that $\det \mathbf{B}_i(t = t_0) > 0$, which is a contradiction with the fact that at least one eigenvalues is zero at $t = t_0$, i.e. $\mathbf{B}_i$ is still positive definite and so $\det \mathbf{B}_i(t = t_0^i) \geq 1$. Thus we find that $\mathbf{B}_i$ is positive definite for all t and

$$\det \mathbf{B}_i(t) \geq 1 \quad i = 1, 2, \ \forall t \geq 0. \tag{18}$$

Further, together with

$$\operatorname{tr} \mathbf{B}_i \geq d(\det(\mathbf{B}_i))^{1/d}, \quad i = 1, 2. \tag{19}$$

we obtain

$$\operatorname{tr} \mathbf{B}_i \geq d. \tag{20}$$

This important result is used in the next section for getting the apriori estimates for generalized Burgers model.

3. Simulations in the deforming domains

We use the models (7), (9), (11) and (16) to simulate flows taking place in domains whose boundaries are deforming. The governing equations for the problems under consideration are written in the Eulerian description.

The problems are solved in the domain Ω_x using the Finite element method that is based on the weak formulation. . For the boundary conditions we assume that the boundary $\partial\Omega_x$ consists of two parts Γ_N and Γ_D such that $\Gamma_N \cup \Gamma_D = \partial\Omega_x$ and $\Gamma_N \cap \Gamma_D = \emptyset$. We suppose that Dirichlet boundary condition $\mathbf{v} = \mathbf{v}_D$ is prescribed on Γ_D and the normal traction $\mathbf{Tn} = \mathbf{t}$ is given on Γ_N.

First we derive apriori estimates, for simplicity, we suppose that $\mathbf{v} = 0$ on whole boundary $\partial\Omega_x$. We multiply balance of linear momentum (2) by $\mathbf{v}$, integrate over Ω_x and use Gauss theorem

$$\frac{\rho}{2}\frac{\mathrm{d}}{\mathrm{d}t}\int_{\Omega_x} |\mathbf{v}|^2 \,\mathrm{d}x = -\int_{\Omega_x} \mathbf{T}\cdot\mathbf{D}\,\mathrm{d}x, \tag{21}$$

then take the trace of (16b) and (16c) and integrate the result over Ω_x

$$\frac{\mathrm{d}}{\mathrm{d}t}\int_{\Omega_x} \operatorname{tr}(\mathbf{B}_1 - \mathbf{I})\,\mathrm{d}x + \frac{1}{\tau_1}\int_{\Omega_x} \operatorname{tr}(\mathbf{B}_1 - \mathbf{I})\,\mathrm{d}x = 2\int_{\Omega_x} \mathbf{B}_1\cdot\mathbf{D}\,\mathrm{d}x\,, \tag{22}$$

$$\frac{\mathrm{d}}{\mathrm{d}t}\int_{\Omega_x} \operatorname{tr}(\mathbf{B}_2 - \mathbf{I})\,\mathrm{d}x + \frac{1}{\tau_2}\int_{\Omega_x} \operatorname{tr}(\mathbf{B}_2 - \mathbf{I})\,\mathrm{d}x = 2\int_{\Omega_x} \mathbf{B}_2\cdot\mathbf{D}\,\mathrm{d}x \tag{23}$$

and sum (21) + $G_1/2 \times$ (22) + $G_2/2 \times$ (23)

$$\begin{aligned}\frac{\rho}{2}\frac{\mathrm{d}}{\mathrm{d}t}\int_{\Omega_x} |\mathbf{v}|^2 \,\mathrm{d}x + \eta\int_{\Omega_x} |\nabla\mathbf{v}|^2 \,\mathrm{d}x + \frac{G_1}{2}\frac{\mathrm{d}}{\mathrm{d}t}\int_{\Omega_x} \operatorname{tr}(\mathbf{B}_1 - \mathbf{I})\,\mathrm{d}x + \frac{G_1}{2\tau_1}\int_{\Omega_x} \operatorname{tr}(\mathbf{B}_1 - \mathbf{I})\,\mathrm{d}x \\ + \frac{G_2}{2}\frac{\mathrm{d}}{\mathrm{d}t}\int_{\Omega_x} \operatorname{tr}(\mathbf{B}_2 - \mathbf{I})\,\mathrm{d}x + \frac{G_2}{2\tau_2}\int_{\Omega_x} \operatorname{tr}(\mathbf{B}_2 - \mathbf{I})\,\mathrm{d}x = 0.\end{aligned} \tag{24}$$

Equation (20) guarantees that all terms are non-negative. Since for $i = 1, 2$, $\mathbf{B}_i$ are symmetric and positive definite, it can be shown that the components are bounded by their trace, i.e. $|(\mathbf{B}_i)_{ij}| \leq \operatorname{tr} \mathbf{B}_i$. Thus we obtain the following apriori estimates

$$\|\mathbf{v}\|_V \leq C, \quad \|\mathbf{B}_1\|_{L^\infty(0,T;L^1(\Omega_x))^{d\times d}} \leq C, \quad \|\mathbf{B}_2\|_{L^\infty(0,T;L^1(\Omega_x))^{d\times d}} \leq C, \tag{25}$$

where $V = L^\infty(0,T;L^2(\Omega_x))^d \cap L^2(0,T;W^{1,2}(\Omega_x))^d$. Since all computations in this paper are done in a two-dimensional space, from now onwards we will assume that $d = 2$. The

estimate for pressure is obtained from the balance of linear momentum, we apply divergence on (2) and get

$$-\Delta p = \operatorname{div}\operatorname{div}\left(\mathbf{v}\otimes\mathbf{v} - 2\eta_s\mathbf{D} - G_1(\mathbf{B}_1-\mathbf{I}) - G_2(\mathbf{B}_2-\mathbf{I})\right) \tag{26}$$

which suggests that pressure p can at most satisfy the following estimate

$$\|p\|_{L^2(0,T;L^1(\Omega_x)} \leq C. \tag{27}$$

Using the apriori estimates the weak renormalized formulation[1] is the following: The quadruple $(\mathbf{v}, p, \mathbf{B}_1, \mathbf{B}_2) \in V\times L^2(0,T;L^1(\Omega_x))\times L^\infty(0,T;L^1(\Omega_x))^{2\times 2}\times L^\infty(0,T;L^1(\Omega_x))^{2\times 2}$, such that $\mathbf{v}-\tilde{\mathbf{v}} \in L^2(0,T;W^{1,2}_{0,\Gamma_D}(\Omega_x))^2$ is a weak renormalized solution of the generalized Burgers model (16) in $\Omega_x \subset \mathbb{R}^2$ if

$$\int_{\Omega_x} \operatorname{tr}(\nabla\mathbf{v}) q \,\mathrm{d}x = 0, \tag{28a}$$

$$\int_{\Omega_x} \rho\left[\frac{\partial\mathbf{v}}{\partial t} + (\nabla\mathbf{v})\mathbf{v}\right]\cdot\mathbf{q}\,\mathrm{d}x - \int_{\Omega_x}\operatorname{div}\mathbf{T}\cdot\mathbf{q}\,\mathrm{d}x = 0, \tag{28b}$$

$$\mathbf{T} = -p\mathbf{I} + \eta_s\left((\nabla\mathbf{v}) + (\nabla\mathbf{v})^{\mathrm{T}}\right) + G_1(\mathbf{B}_1-\mathbf{I}) + G_2(\mathbf{B}_2-\mathbf{I}), \tag{28c}$$

$$\begin{aligned}\int_{\Omega_x}\left[\frac{\partial\mathbf{R}_1^L(\mathbf{B}_1)}{\partial t} + \left(-(\nabla\mathbf{v})\mathbf{B}_1 - \mathbf{B}_1(\nabla\mathbf{v})^{\mathrm{T}} + \frac{1}{\tau_1}(\mathbf{B}_1-\mathbf{I})\right)\circ(\mathbf{R}_1^L)'(\mathbf{B}_1)\right]\cdot\mathbf{Q}_1\,\mathrm{d}x \\ - \int_{\Omega_x}\mathbf{R}_1^L(\mathbf{B}_1)\otimes\mathbf{v}\cdot\nabla\mathbf{Q}_1\,\mathrm{d}x + \int_{\partial\Omega_x}(\mathbf{v}\cdot\mathbf{n})\,\mathbf{R}_1^L(\mathbf{B}_1)\cdot\mathbf{Q}_1\,\mathrm{d}S = 0,\end{aligned} \tag{28d}$$

$$\begin{aligned}\int_{\Omega_x}\left[\frac{\partial\mathbf{R}_2^L(\mathbf{B}_2)}{\partial t} + \left(-(\nabla\mathbf{v})\mathbf{B}_2 - \mathbf{B}_2(\nabla\mathbf{v})^{\mathrm{T}} + \frac{1}{\tau_2}(\mathbf{B}_2-\mathbf{I})\right)\circ(\mathbf{R}_2^L)'(\mathbf{B}_2)\right]\cdot\mathbf{Q}_2\,\mathrm{d}x \\ - \int_{\Omega_x}\mathbf{R}_2^L(\mathbf{B}_2)\otimes\mathbf{v}\cdot\nabla\mathbf{Q}_2\,\mathrm{d}x + \int_{\partial\Omega_x}(\mathbf{v}\cdot\mathbf{n})\,\mathbf{R}_2^L(\mathbf{B}_2)\cdot\mathbf{Q}_2\,\mathrm{d}S = 0\end{aligned} \tag{28e}$$

is satisfied for all $(q, \mathbf{q}, \mathbf{Q}_1, \mathbf{Q}_2) \in C^1(\Omega_x)\times V_1\times C^1(\Omega_x)^{2\times 2}\times C^1(\Omega_x)^{2\times 2}$, all $\mathbf{R}_i^L \in \mathcal{R}$ and a.a. $t\in(0,T)$, where $V_1 = \{\mathbf{v}\in C^\infty(\Omega_x)^2, \mathbf{v}=\mathbf{0} \text{ on } \Gamma_D\}$ and $\tilde{\mathbf{v}}|_{\Gamma_D} = \mathbf{v}_D$. Further,

$$\mathbf{A}\circ\mathbf{B} = \begin{pmatrix} A_{11}B_{11} & A_{12}B_{12} \\ A_{21}B_{21} & A_{22}B_{22}\end{pmatrix} \tag{29}$$

is the Hadamard product of two matrices. We define $\mathbf{R}^L(\mathbf{B}) \in \mathcal{R}$ as a set of continuously differentiable matrix functions in the form

$$\mathbf{R}^L(\mathbf{B}) = \begin{pmatrix} R_{11}^L(B_{11}) & R_{12}^L(B_{12}) \\ R_{21}^L(B_{21}) & R_{22}^L(B_{22})\end{pmatrix}, \quad (\mathbf{R}^L)'(\mathbf{B}) = \begin{pmatrix} \frac{\partial R_{11}^L}{\partial B_{11}} & \frac{\partial R_{12}^L}{\partial B_{12}} \\ \frac{\partial R_{21}^L}{\partial B_{21}} & \frac{\partial R_{22}^L}{\partial B_{22}},\end{pmatrix} \tag{30}$$

where

$$\begin{aligned}\mathcal{R} = \big\{&(R_{ij}^L)_{i,j=1}^2 \text{ is a continuously differentiable matrix function of } B_{ij}, R_{ij}^L(B_{ij}) = B_{ij} \\ &\text{for } |B_{ij}|\leq L \text{ and } R_{ij}^L(B_{ij}) = L+1 \text{ for } |B_{ij}|> L+1,\ L=2,\dots,\infty\big\}.\end{aligned}$$

[1]The weak renormalized formulation is obtained by taking the Hadamard product of (16b), resp. (16c) with $(\mathbf{R}_1^L)'(\mathbf{B}_1)$, resp. $(\mathbf{R}_2^L)'(\mathbf{B}_2)$ that are defined later in text. The Gauss theorem is applied on the convective term in (16b), and (16c).

For numerical implementation all computations are carried out for $R^L_{ij}(B_{ij}) = B_{ij}$ with the original convective term, then the weak formulation of Eulerian description of (16) is in the form[2]

$$\int_{\Omega_x} \operatorname{tr}(\nabla \mathbf{v}) q \,\mathrm{d}x = 0, \tag{31a}$$

$$\int_{\Omega_x} \rho \left[\frac{\partial \mathbf{v}}{\partial t} + (\nabla \mathbf{v})\mathbf{v} \right] \cdot \mathbf{q} \,\mathrm{d}x - \int_{\Omega_x} \operatorname{div} \mathbf{T} \cdot \mathbf{q} \,\mathrm{d}x = 0, \tag{31b}$$

$$\mathbf{T} = -p\mathbf{I} + \eta_s \left((\nabla \mathbf{v}) + (\nabla \mathbf{v})^{\mathrm{T}} \right) + G_1(\mathbf{B}_1 - \mathbf{I}) + G_2(\mathbf{B}_2 - \mathbf{I}), \tag{31c}$$

$$\int_{\Omega_x} \left[\frac{\partial \mathbf{B}_1}{\partial t} + (\nabla \mathbf{B}_1)\mathbf{v} - (\nabla \mathbf{v})\mathbf{B}_1 - \mathbf{B}_1(\nabla \mathbf{v})^{\mathrm{T}} + \frac{1}{\tau_1}(\mathbf{B}_1 - \mathbf{I}) \right] \cdot \mathbf{Q}_1 \,\mathrm{d}x = 0, \tag{31d}$$

$$\int_{\Omega_x} \left[\frac{\partial \mathbf{B}_2}{\partial t} + (\nabla \mathbf{B}_2)\mathbf{v} - (\nabla \mathbf{v})\mathbf{B}_2 - \mathbf{B}_2(\nabla \mathbf{v})^{\mathrm{T}} + \frac{1}{\tau_2}(\mathbf{B}_2 - \mathbf{I}) \right] \cdot \mathbf{Q}_2 \,\mathrm{d}x = 0. \tag{31e}$$

Eulerian formulation is not suited for describing the problem in deforming boundaries. Our aim is to solve the problem in a fixed domain by transforming the equations from the deforming Eulerian domain to a fixed domain. To do this we use the arbitrary Lagrangian-Eulerian (ALE) formulation. Before we do that we show how we can obtain the equations in the simpler case using the Lagrangian formulation for problems where no inflow or outflow takes place. Both Lagrangian and ALE formulation are derived for the generalized Burgers model (16).

3.1. Lagrangian formulation

We identify the fixed computational mesh with the reference Lagrangian configuration Ω_X which is mapped into the current Eulerian configuration Ω_x by

$$\varphi : X \to x := X + \mathbf{u}. \tag{32}$$

The velocity $\mathbf{v}$ is defined by

$$\mathbf{v} := \frac{\partial \varphi}{\partial t}\Big|_X = \frac{\partial \mathbf{u}}{\partial t}, \tag{33}$$

the deformation gradient $\mathbf{F}$ and its Jacobian J are defined as

$$\mathbf{F} = \frac{\partial \varphi}{\partial X} = \mathbf{I} + \nabla_X \mathbf{u}, \quad J = \det \mathbf{F}. \tag{34}$$

We want to solve the problem on the fixed mesh corresponding to the domain Ω_X where all the unknowns live. We use a monolithic approach and solve the problem as one big coupled system of equations including the equation for the deformation of the mesh (32).

We transform the Eulerian weak formulation (31) into the Lagrangian by substituting all derivatives with respect to x to derivatives with respect to X. We need to transform the

[2]This is not a standard weak formulation, here the divergence theorem is not used in the balance of linear momentum.

velocity gradient $\nabla_x \mathbf{v}$ and the material time derivatives, i.e.

$$\nabla_X \mathbf{v} = \frac{\partial \mathbf{v}(\varphi(X,t),t)}{\partial X} = \frac{\partial \mathbf{v}}{\partial x}\frac{\partial \varphi}{\partial X} = (\nabla_x \mathbf{v})\mathbf{F} \quad \Rightarrow \quad \nabla_x \mathbf{v} = (\nabla_X \mathbf{v})\mathbf{F}^{-1} \tag{35}$$

and the material time derivatives of scalar α

$$\frac{\partial \alpha}{\partial t}\Big|_X = \frac{\mathrm{d}\alpha(\varphi(X,t),t)}{\mathrm{d}t}\Big|_X = \frac{\partial \alpha}{\partial t}\Big|_x + \frac{\partial \alpha}{\partial x}\frac{\partial \varphi}{\partial t}\Big|_X = \frac{\partial \alpha}{\partial t}\Big|_x + \mathbf{v}\cdot\nabla_x \alpha. \tag{36}$$

Further, the integrals over Ω_x are transformed to the integrals over Ω_X by using the integral substitution theorem. The last tool that is used in the balance of linear momentum is the Piola identity that states that $\mathrm{div}_X\left((\det \mathbf{F})\mathbf{F}^{-\mathrm{T}}\right) = 0$. Let us compute the $\mathrm{div}_x \mathbf{T}$ term in the weak formulation

$$\int_{\Omega_x} \mathrm{div}_x \mathbf{T}\cdot\mathbf{q}\,\mathrm{d}x = \int_{\Omega_X} J(\nabla_X \mathbf{T})\mathbf{F}^{-\mathrm{T}}\cdot\mathbf{q}\,\mathrm{d}X = \int_{\Omega_X}\left(J(\nabla_X \mathbf{T})\mathbf{F}^{-\mathrm{T}} + \mathbf{T}\underbrace{\mathrm{div}_X\left(J\mathbf{F}^{-\mathrm{T}}\right)}_{0}\right)\cdot\mathbf{q}\,\mathrm{d}X = \int_{\Omega_X}\mathrm{div}_X(J\mathbf{T}\mathbf{F}^{-\mathrm{T}})\cdot\mathbf{q}\,\mathrm{d}X. \tag{37}$$

Using the weak formulation (31) the Eulerian description in Ω_x is transformed into the Lagrangian description in Ω_X

$$\int_{\Omega_X} J\,\mathrm{tr}\left((\nabla_X \mathbf{v})\mathbf{F}^{-1}\right) q\,\mathrm{d}X = 0, \tag{38}$$

$$\int_{\Omega_X} J\rho\frac{\partial \mathbf{v}}{\partial t}\cdot\mathbf{q}\,\mathrm{d}X - \int_{\Omega_X}\mathrm{div}_X\left(J\mathbf{T}\mathbf{F}^{-T}\right)\cdot\mathbf{q}\,\mathrm{d}X = 0, \tag{39}$$

$$\mathbf{T} = -p\mathbf{I} + \eta_s\left((\nabla_X \mathbf{v})\mathbf{F}^{-1} + \mathbf{F}^{-\mathrm{T}}(\nabla_X \mathbf{v})^{\mathrm{T}}\right) + G_1(\mathbf{B}_1 - \mathbf{I}) + G_2(\mathbf{B}_2 - \mathbf{I}), \tag{40}$$

$$\int_{\Omega_X} J\left(\frac{\partial \mathbf{B}_1}{\partial t} - (\nabla_X \mathbf{v})\mathbf{F}^{-1}\mathbf{B}_1 - \mathbf{B}_1\mathbf{F}^{-\mathrm{T}}(\nabla_X \mathbf{v})^{\mathrm{T}} + \frac{1}{\tau_1}(\mathbf{B}_1 - \mathbf{I})\right)\cdot\mathbf{Q}_1\,\mathrm{d}X = 0, \tag{41}$$

$$\int_{\Omega_X} J\left(\frac{\partial \mathbf{B}_2}{\partial t} - (\nabla_X \mathbf{v})\mathbf{F}^{-1}\mathbf{B}_2 - \mathbf{B}_2\mathbf{F}^{-\mathrm{T}}(\nabla_X \mathbf{v})^{\mathrm{T}} + \frac{1}{\tau_2}(\mathbf{B}_2 - \mathbf{I})\right)\cdot\mathbf{Q}_2\,\mathrm{d}X = 0. \tag{42}$$

We need to add equation (33) to close the system of equations (unknown $\mathbf{u}$ is hidden in $\mathbf{F}$ and J).

The above formulation can be used if the changes in the domain are not too big. The main problem is in virtue of the fact that all points in the domain are material points and for example vortices in the flow can damage the deformed mesh[3]. Such an example can be seen in Figure 1.

3.2. Arbitrary Lagrangian-Eulerian formulation

In view of such difficulties with the purely Lagrangian formulation, we choose to use the ALE formulation which does not present such difficulties (for more details, see for example

[3]Here a monolithic approach with a fixed mesh is used, the deformation of the mesh is computed by (32). The damage of the mesh is a consequence of the fact that the consecutive set of linear equations creates a singular matrix.

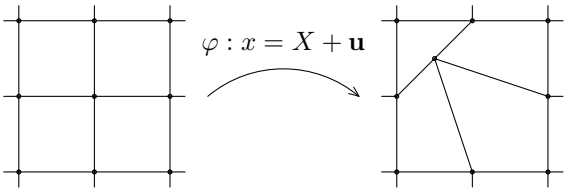

Figure 1: Damaged mesh in the case of Lagrangian formulation.

lecture notes by Scovazzi and Hughes [17]). Instead of identifying the mesh with the Lagrangian domain Ω_X we identify it with a new domain Ω_χ (see Figure 2), where $\hat{\varphi}$ maps Ω_χ into Ω_x by

$$\hat{\varphi} : \chi \to x := \chi + \hat{\mathbf{u}}, \tag{43}$$

where $\hat{\mathbf{u}}$ is an arbitrary deformation (i.e. the deformation of the mesh). If the time derivative of $\hat{\mathbf{u}}$ was equal to the velocity $\mathbf{v}$ then all points would be the material points, $\Omega_\chi = \Omega_X$ and we would obtain the Lagrange formulation. Instead of this we only require to have the material points on the boundary $\partial\Omega_\chi$, inside the domain Ω_χ we just need to have a unique solution for $\hat{\mathbf{u}}$, for simplicity we use a Laplace equation, i.e.

$$\hat{\mathbf{u}} = \begin{cases} \dfrac{\partial \hat{\mathbf{u}}}{\partial t} = \mathbf{v} \quad \text{on } \partial\Omega_\chi \\ \\ -\Delta_\chi \hat{\mathbf{u}} = 0 \quad \text{inside } \Omega_\chi. \end{cases} \tag{44}$$

We define the deformation gradient and its Jacobian by

$$\hat{\mathbf{F}} = \frac{\partial \hat{\varphi}}{\partial \chi} = \mathbf{I} + \nabla_\chi \hat{\mathbf{u}}, \quad \hat{J} = \det \hat{\mathbf{F}}. \tag{45}$$

The same procedure as in the Lagrangian case is used to transform (31) from Ω_x to Ω_χ. The velocity gradient transforms in the same way as before

$$\nabla_\chi \mathbf{v} = \frac{\partial \mathbf{v}(\varphi(\chi,t),t)}{\partial \chi} = \frac{\partial \mathbf{v}}{\partial x}\frac{\partial \hat{\varphi}}{\partial \chi} = (\nabla_x \mathbf{v})\hat{\mathbf{F}} \quad \Rightarrow \quad \nabla_x \mathbf{v} = (\nabla_\chi \mathbf{v})\hat{\mathbf{F}}^{-1}. \tag{46}$$

The transformation of the material time derivative is more difficult, first we compute

$$\frac{\partial \alpha}{\partial t}\Big|_\chi = \frac{\mathrm{d}\alpha(\hat{\varphi}(\chi,t),t)}{\mathrm{d}t}\Big|_\chi = \frac{\partial \alpha}{\partial t}\Big|_x + \frac{\partial \alpha}{\partial x}\frac{\partial \hat{\varphi}}{\partial t}\Big|_\chi = \frac{\partial \alpha}{\partial t}\Big|_x + \frac{\partial \hat{\mathbf{u}}}{\partial t} \cdot \nabla_x \alpha. \tag{47}$$

Using (47) we obtain

$$\begin{aligned} \frac{\partial \alpha}{\partial t}\Big|_x + \mathbf{v} \cdot \nabla_x \alpha &= \frac{\partial \alpha}{\partial t}\Big|_\chi + \left(\mathbf{v} - \frac{\partial \hat{\mathbf{u}}}{\partial t}\right) \cdot \nabla_x \alpha \\ &= \frac{\partial \alpha}{\partial t}\Big|_\chi + \left(\mathbf{v} - \frac{\partial \hat{\mathbf{u}}}{\partial t}\right) \cdot (\nabla_\chi \alpha)\hat{\mathbf{F}}^{-1} \\ &= \frac{\partial \alpha}{\partial t}\Big|_\chi + \left(\hat{\mathbf{F}}^{-1}\left(\mathbf{v} - \frac{\partial \hat{\mathbf{u}}}{\partial t}\right)\right) \cdot \nabla_\chi \alpha. \end{aligned} \tag{48}$$

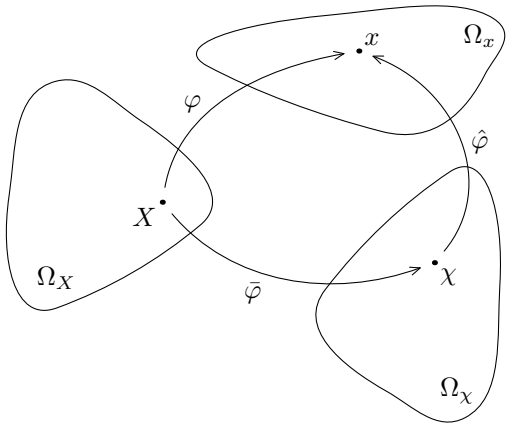

Figure 2: ALE formulation.

Using (46), (48), the integral substitution theorem and Piola identity as in the Lagrangian case we transform the weak formulation (31) to

$$\int_{\Omega_\chi} \hat{J} \operatorname{tr}\left((\nabla_\chi \mathbf{v})\hat{\mathbf{F}}^{-1}\right) q \,\mathrm{d}\chi = 0, \tag{49a}$$

$$\int_{\Omega_\chi} \hat{J}\rho \left[\frac{\partial \mathbf{v}}{\partial t} + (\nabla_\chi \mathbf{v})\left(\hat{\mathbf{F}}^{-1}\left(\mathbf{v} - \frac{\partial \hat{\mathbf{u}}}{\partial t}\right)\right)\right] \cdot \mathbf{q} \,\mathrm{d}\chi - \int_{\Omega_\chi} \operatorname{div}_\chi\left(\hat{J}\hat{\mathbf{T}}\hat{\mathbf{F}}^{-T}\right) \cdot \mathbf{q} \,\mathrm{d}\chi = 0, \tag{49b}$$

$$\hat{\mathbf{T}} = -p\mathbf{I} + \eta_s\left((\nabla_\chi \mathbf{v})\hat{\mathbf{F}}^{-1} + \hat{\mathbf{F}}^{-\mathrm{T}}(\nabla_\chi \mathbf{v})^{\mathrm{T}}\right) + G_1(\mathbf{B}_1 - \mathbf{I}) + G_2(\mathbf{B}_2 - \mathbf{I}), \tag{49c}$$

$$\int_{\Omega_\chi} \hat{J}\left[\frac{\partial \mathbf{B}_1}{\partial t} + (\nabla_\chi \mathbf{B}_1)\left(\hat{\mathbf{F}}^{-1}\left(\mathbf{v} - \frac{\partial \hat{\mathbf{u}}}{\partial t}\right)\right)\right.$$
$$\left. -(\nabla_\chi \mathbf{v})\hat{\mathbf{F}}^{-1}\mathbf{B}_1 - \mathbf{B}_1\hat{\mathbf{F}}^{-\mathrm{T}}(\nabla_\chi \mathbf{v})^{\mathrm{T}} + \frac{1}{\tau_1}(\mathbf{B}_1 - \mathbf{I})\right] \cdot \mathbf{Q}_1 \,\mathrm{d}\chi = 0, \tag{49d}$$

$$\int_{\Omega_\chi} \hat{J}\left[\frac{\partial \mathbf{B}_2}{\partial t} + (\nabla_\chi \mathbf{B}_2)\left(\hat{\mathbf{F}}^{-1}\left(\mathbf{v} - \frac{\partial \hat{\mathbf{u}}}{\partial t}\right)\right)\right.$$
$$\left. -(\nabla_\chi \mathbf{v})\hat{\mathbf{F}}^{-1}\mathbf{B}_2 - \mathbf{B}_2\hat{\mathbf{F}}^{-\mathrm{T}}(\nabla_\chi \mathbf{v})^{\mathrm{T}} + \frac{1}{\tau_2}(\mathbf{B}_2 - \mathbf{I})\right] \cdot \mathbf{Q}_2 \,\mathrm{d}\chi = 0. \tag{49e}$$

This set of equations is closed with the equation (44) with the weak formulation

$$\int_{\Omega_\chi} \nabla_\chi \hat{\mathbf{u}} \cdot \nabla_\chi \mathbf{t} \,\mathrm{d}\chi = 0. \tag{50}$$

3.3. Finite element method for ALE formulation

In order to compute problems involving deforming domains numerically, a discrete approximation has to be created, here the Finite element method is used. It is based on the weak formulation consisting of (49) and (50) with one difference in the balance of linear momentum where the divergence theorem is used

$$\int_{\Omega_\chi} \hat{J}\rho \left[\frac{\partial \mathbf{v}}{\partial t} + (\nabla_\chi \mathbf{v})\left(\hat{\mathbf{F}}^{-1}\left(\mathbf{v} - \frac{\partial \hat{\mathbf{u}}}{\partial t}\right)\right)\right] \cdot \mathbf{q} \,\mathrm{d}\chi = -\int_{\Omega_\chi} \hat{J}\hat{\mathbf{T}}\hat{\mathbf{F}}^{-T} \cdot \nabla_\chi \mathbf{q} \,\mathrm{d}\chi + \int_{\partial\Omega_\chi} \left(\hat{J}\hat{\mathbf{T}}\hat{\mathbf{F}}^{-T}\right)\mathbf{n}_\chi \cdot \mathbf{q} \,\mathrm{d}S_\chi, \tag{51}$$

where $\mathbf{n}_\chi$ is the outer unit normal vector in the domain Ω_χ. The last term in (51) is used for prescribing the Neumann boundary condition. To be precise, we prescribe $\left(\hat{J}\hat{\mathbf{T}}\hat{\mathbf{F}}^{-T}\right)\mathbf{n}_\chi$ as a force acting on the part of boundary $\partial\Omega_\chi$. This means that we prescribe a vector whose components are perpendicular/parallel with the normal vector in the actual configuration and so we can easily push the material perpendicular to the boundary. For the sake of simplicity, when we discuss the boundary conditions later in the text instead of writing the component $(\hat{J}\hat{\mathbf{T}}\hat{\mathbf{F}}^{-T})_{ij}$ we will write the component as T_{ij}.

3.3.1. Time discretization

Time derivatives in (49) are implicitly fully mixed (see for example the transformed convective terms). Let us consider the following differential equation for y

$$\frac{\partial y(x,t)}{\partial t} + f\left(y(x,t), \frac{\partial y(x,t)}{\partial t}\right) = 0 \text{ in } \Omega \times [0,T], \tag{52}$$

then the time derivatives are discretized by two different time schemes:

Implicit backward Euler scheme The first order unconditionally stable time scheme.

$$\frac{y^{n+1}(x) - y^n(x)}{\Delta t^n} + f\left(y^{n+1}(x), \frac{y^{n+1}(x) - y^n(x)}{\Delta t^n}\right), \tag{53}$$

where Δt^n is the $n-$th time step, $y^{n+1}(x) = y(x, t_0 + \sum_{i=0}^{n} \Delta t^i)$ and on every $(n+1)$-th time level the space problem is solved using FEM.

We found out that this first order scheme is not satisfactory for computing these problems and so a higher order scheme has to be used. However, it is not clear how for example the Crank-Nicholson time scheme should be implemented in case of this implicitly fully mixed time derivatives. That is why we used the higher order time scheme (almost third order) proposed by Glowinski [18] and tested by Turek et al. [19].

Implicit Glowinski three step scheme This time scheme consists in two implicit Euler steps and one explicit step, we define $\theta := 1 - 1/\sqrt{2}$:

1. $\dfrac{y^{n+\theta}(x) - y^n(x)}{\theta\Delta t^n} = f\left(y^{n+\theta}(x)), \dfrac{y^{n+\theta}(x) - y^n(x)}{\theta\Delta t^n}\right),$
2. $y^{n+1-\theta} = \dfrac{1-\theta}{\theta} y^{n+\theta} + \dfrac{2\theta - 1}{\theta} y^n,$
3. $\dfrac{y^{n+1}(x) - y^{n+1-\theta}(x)}{\theta\Delta t^n} = f\left(y^{n+1}(x)), \dfrac{y^{n+1}(x) - y^{n+1-\theta}(x)}{\theta\Delta t^n}\right).$

At every step the space problem is solved using FEM.

3.3.2. Space discretization

The domain Ω_χ is approximated by Ω_h with a polygonal boundary. Ω_h is discretized by regular quadrilaterals T belonging to $\mathcal{T}_h$ that is regular in the sense that any two quadrilaterals are disjoint or have a common vertex or a common edge.

Pressure p / velocity $\mathbf{v}$ / deformation $\hat{\mathbf{u}}$ / parts of the tensors $\mathbf{B}_1$ and $\mathbf{B}_2$ are approximated by P_1^{disc} / Q_2 / Q_2 / Q_2 / Q_2 elements[4]. The combination of Q_2 for the velocity and P_1^{disc} for the pressure is a stable pair for velocity and pressure satisfying the Babuška-Brezi condition in the case of the incompressible Navier-Stokes equations, Q_2 for the parts $\mathbf{B}_1$ and $\mathbf{B}_2$ is not probably optimal, but it works.

We utilize a fully coupled monolithic finite element approach that treats all the numerical variables simultaneously. At each time level the standard Galerkin method is used, the obtained set of non-linear algebraic equations is solved by Newton's method. The set of linear equations in every iteration of the Newton's method is solved by two linear solvers depending on the size of the problem. For the smaller problems the direct solver UMFPACK by Davis [20] is used, for the biggest problem the iterative solver GMRES with ILU1 preconditioning from the package SPLIB by Bramley [21] is used. The implementation is based on the code developed by Hron [22].

In the rest of the paper we compute three problems that differ only in the domain and the boundary conditions. In all problems the material is at rest at $t = 0$, the initial conditions are

$$p(0) = 0, \quad \hat{\mathbf{u}}(0) = \mathbf{0}, \quad \mathbf{v}(0) = \mathbf{0}, \quad \mathbf{B}_1(0) = \mathbf{B}_2(0) = \mathbf{I}. \tag{54}$$

The boundary conditions are different in each problem, but all problems have the same Dirichlet boundary condition given by (44)

$$\frac{\partial \hat{\mathbf{u}}}{\partial t} = \mathbf{v} \text{ on } \partial\Omega.$$

The convergence and mesh stability analysis is carried out only for the first problem, otherwise all problems are computed with constant time step $\Delta t = 0.01$ s and the mesh depicted. All meshes are locally refined near the boundary.

4. Solution of the boundary-initial boundary value problems

4.1. Problem 1 – Response of the viscoelastic models in a benchmark problem

In the first problem we delineate the response of the four viscoelastic models presented in the Section 2 and show how the solution depends on material parameters that characterize the materials.

Let us consider a rectangular piece of material, see Figure 3. The width is 3m, the height is 1m.[5] The material is placed on the ground where it can fully slip in the x-direction, but it can not move in the y-direction. All other sides of the rectangle can freely move.

We ignore the effect of gravity. At the beginning the material is in rest and does not move. Suddenly at time $t = 0$ the body is pushed at the top by a constant traction vector that results in the component of the stress tensor $T_{yy} = -5000$ Pa. This stress acts till the time $t = 0.5$ s, and then it suddenly ceases to exist. We observe how the boundary continues to deform after the applied traction ceases.

[4] Q_2 stands for a continuous biquadratic element, P_1^{disc} for a discontinuous linear element.

[5] When non-dimensionalized, this would mean that the width is thrice as much as the thickness. Later, we shall use much thinner domains as an application we have in mind are pavements which are usually modeled as rate type viscoelastic fluids, which are much wider than thick.

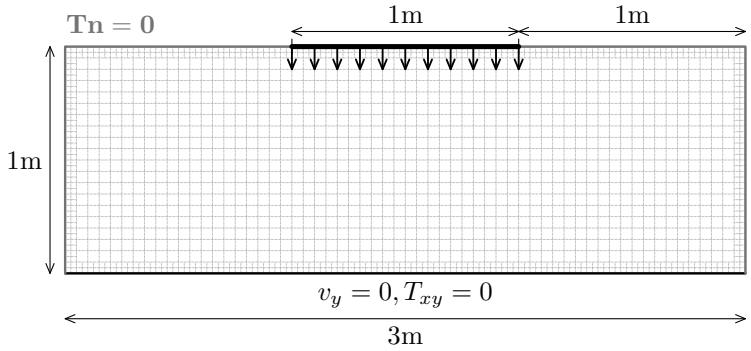

Figure 3: Problem 1.

Model	η_s [Pa s]	τ_1 [s]	τ_2 [s]	G_1 [kPa]	G_2 [kPa]
Maxwell (7)	—	0.2	—	15.0	—
	—	0.8	—	15.0	—
	—	2.0	—	15.0	—
Oldroyd (9)	100.0	0.2	—	15.0	—
	100.0	0.8	—	15.0	—
	100.0	2.0	—	15.0	—
Burgers (11)	—	0.2	2.0	10.0	5.0
N-Burgers (16)	100.0	0.2	2.0	10.0	5.0

Table 1: Material parameters used in the simulation for each model.

The boundary conditions are:

Bottom Dirichlet: $v_y = 0$, Neumann: $T_{xy} = 0$

Top and sides Neumann: $\mathbf{Tn} = \mathbf{0}$, during the pressing $T_{yy} = -5000$ Pa on a part of the boundary.

The material parameters used in the simulation are provided in the Table 1. In the case of the model with only one relaxation time τ and one elastic modulus G, τ_1 and G_1 is used. Density $\rho = 1000$ kg/m^3 in all cases.

In case of the Burgers model given by (11), the two relaxation times are $\tau = 0.2$ and $\tau = 2.0$. The elastic moduli G_1 and G_2 in (11) determine the weights corresponding to the relaxation times τ_1 and τ_2. The more G_1 is higher than G_2, the more the material behaves as a material with the relaxation time τ_1 as the dominant relaxation time. That is why we also use a Maxwell model with relaxation time $\tau = 0.8$ s which is a weighted average in the sense

$$\tau = \frac{G_1\tau_1 + G_2\tau_2}{G_1 + G_2}.$$

We will see that the steady solution for the Maxwell model with this averaged relaxation time and the Burgers model (11) is almost the same.

We carried out the full simulations for all materials listed in Table 1 and we have a fully dynamic movie of the response of each of these materials from which we have picked five snapshots of the deformation of the top side (lateral sides are not depicted). Figure 4 depicts how the y-component of the deformation at the center line depends on time. Vertical lines in the graph denote the times when the snapshots are captured: 0.53s (minimum for Burgers' models), 0.7s, 0.94s (maximum for Maxwell and Oldroyd-B with $\tau = 2.0$ s) and 1.14s (maximum for Burgers' models). The snapshots are depicted in the Figure 5.

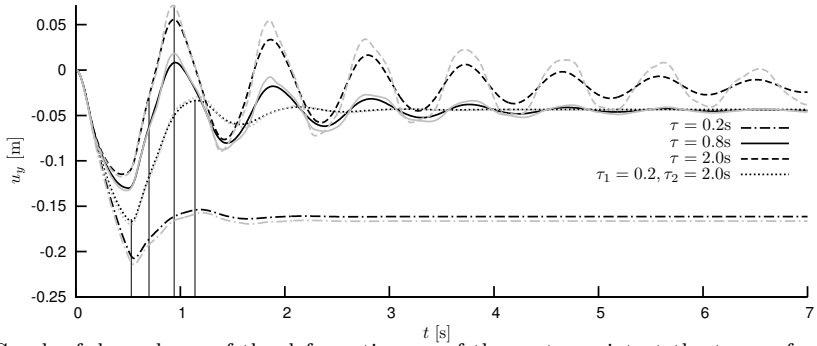

Figure 4: Graph of dependence of the deformation u_y of the center point at the top surface with time t, the grey lines correspond to the models with zero Newtonian viscosity (i.e. Maxwell model (7) and Burgers' model (11)). Vertical lines: 0.53s, 0.7s, 0.94s, 1.14s.

The graph shows that the models with zero Newtonian viscosity (i.e. Maxwell model (7) and Burgers' model (11)) are more elastic and oscillate more than the models with corresponding non-zero Newtonian viscosity. Further Oldroyd-B/Maxwell models with relaxation time $\tau = 2.0$ s exhibit both elasticity and damping, and the material with relaxation time $\tau = 0.8$ s exhibit similar behavior but with less elasticity (or with more damping). The material having a relaxation time $\tau = 0.2$ s behaves mostly like a fluid, on pressing the top surface there is only one small wave and the material remains deformed. The most interesting response characteristics are exhibited by the Burgers' models with relaxation times $\tau_1 = 0.2$ s, $\tau_2 = 2.0$ s, in that the displacement after an initial oscillation remains essentially constant.

All the simulations were carried out upto the time $t = 40.0$ s when even the viscoelastic fluid with the greatest elastic response ceases to deform further.

The snapshots in the Figure 5 show that in the case Oldroyd-B model with $\tau = 2.0$ s the shape of the surface is almost concave compared to the other materials. Further it can be seen that at time 40.0 s when all materials cease to deform, the deformations of Burgers' model with $\tau_1 = 0.2$ s, $\tau_2 = 2.0$ s and Oldroyd-B model with $\tau = 0.8$ s are almost the same (dotted line merges the dot-and-dashed line), that is, asymptotically in time both these models have the same response, though their transient response is different. However, it is interesting to note that the relaxation time for the Oldroyd-B model does not equal either of the two relaxation times associated with the Burgers model but in fact has a relaxation time that is inbetween the two values. The specific deformations corresponding to the two models are not of great interest, what is more important is to observe how the deformation takes place and reaches an asymptotic limit in time.

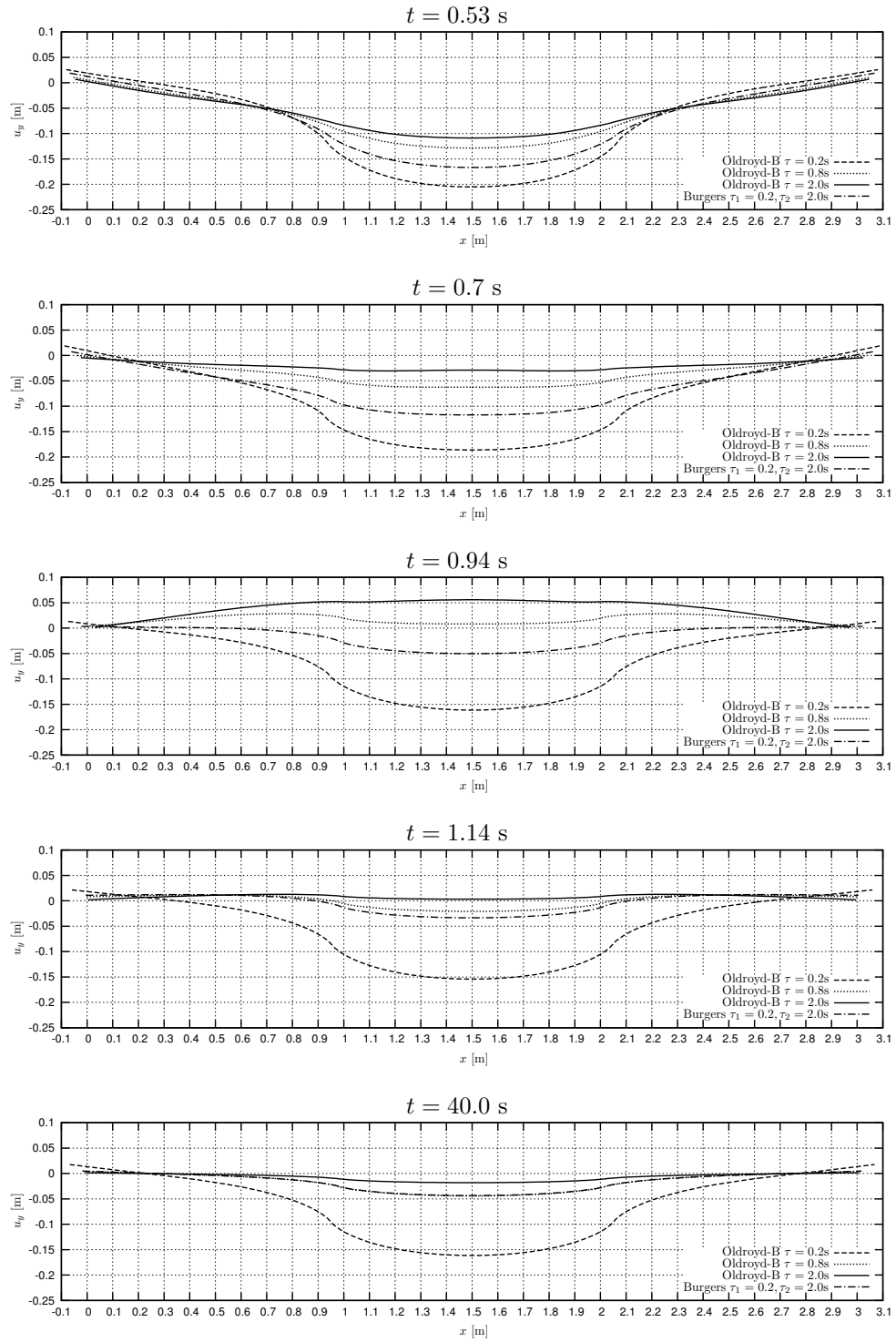

Figure 5: Snapshots of the top side at five different times for Oldroyd-B model and Burgers' model.

4.1.1. Convergence and mesh stability analysis

To verify that our simulations are correct we computed this problem with Oldroyd-B model (9) with $\tau = 0.8$ s on four different meshes (see Table 2) and with four different time steps. All meshes are locally refined near the boundary, in the Table 2 we provide the dimensions of the mesh before the local refinement. The mesh size h is computed from the refined elements. Table 2 also contains information about the dimension of the system of linear equations and the solver that was used.

	mesh dimension	mesh size h	$1/h$	# DOFs	lin. solver
mesh1	15×5	0.1	10	6 016	umfpack
mesh2	30×10	0.05	20	16 991	umfpack
mesh3	60×20	0.025	40	52 891	umfpack
mesh4	120×40	0.0125	80	180 491	gmres

Table 2: Parameters for the meshes used, corresponding number of degrees of freedom and the linear solver that was used.

We computed the problem with four different constant times steps: 0.05, 0.02, 0.01 and 0.005 s (CPU time on mesh4 with $\Delta t = 0.0005$ s was 16 days). We had to use a higher order Glowinski time scheme described in the previous section because the first order backward Euler scheme was not accurate enough. We compared the deformation u_y in the middle of the top side and the kinetic energy of the whole body

$$E_k = \int_{\Omega_x} \frac{1}{2}\rho|\mathbf{v}|^2 \,\mathrm{d}x = \int_{\Omega_\chi} \hat{J}\frac{1}{2}\rho|\mathbf{v}|^2 \,\mathrm{d}\chi$$

at time $t = 0.6$ s (0.1 s after the release of the force) and time $t = 20$ s when the material with this relaxation time is almost at rest[6], see Tables 3, 4 and 5.

mesh\timestep	0.05	0.02	0.01	0.005
mesh1	-0.10926	-0.10857	-0.10852	-0.10851
mesh2	-0.10675	-0.10603	-0.10598	-0.10597
mesh3	-0.10604	-0.10531	-0.10526	-0.10525
mesh4	-0.10573	-0.10498	-0.10493	-0.10492

Table 3: Deformation u_y at the middle of the top surface at $t = 0.6$ s for all four meshes and all four time steps with Glowinski time scheme.

Using these data we computed the relative error related to the value obtained with the smallest time step $\Delta t = 0.005$ s and the densest mesh4. We have plotted the dependence of the relative error on the mesh size h and the time step Δt in Figures 6 (a) – (f) in log-log scale.

The graphs show that the relative error is decreasing with the mesh size h and the time step Δt, and the experimental order of convergence with regard to space is between h and

[6]Kinetic energy E_k is not compared at $t = 20$ s because it is numerically equal to zero.

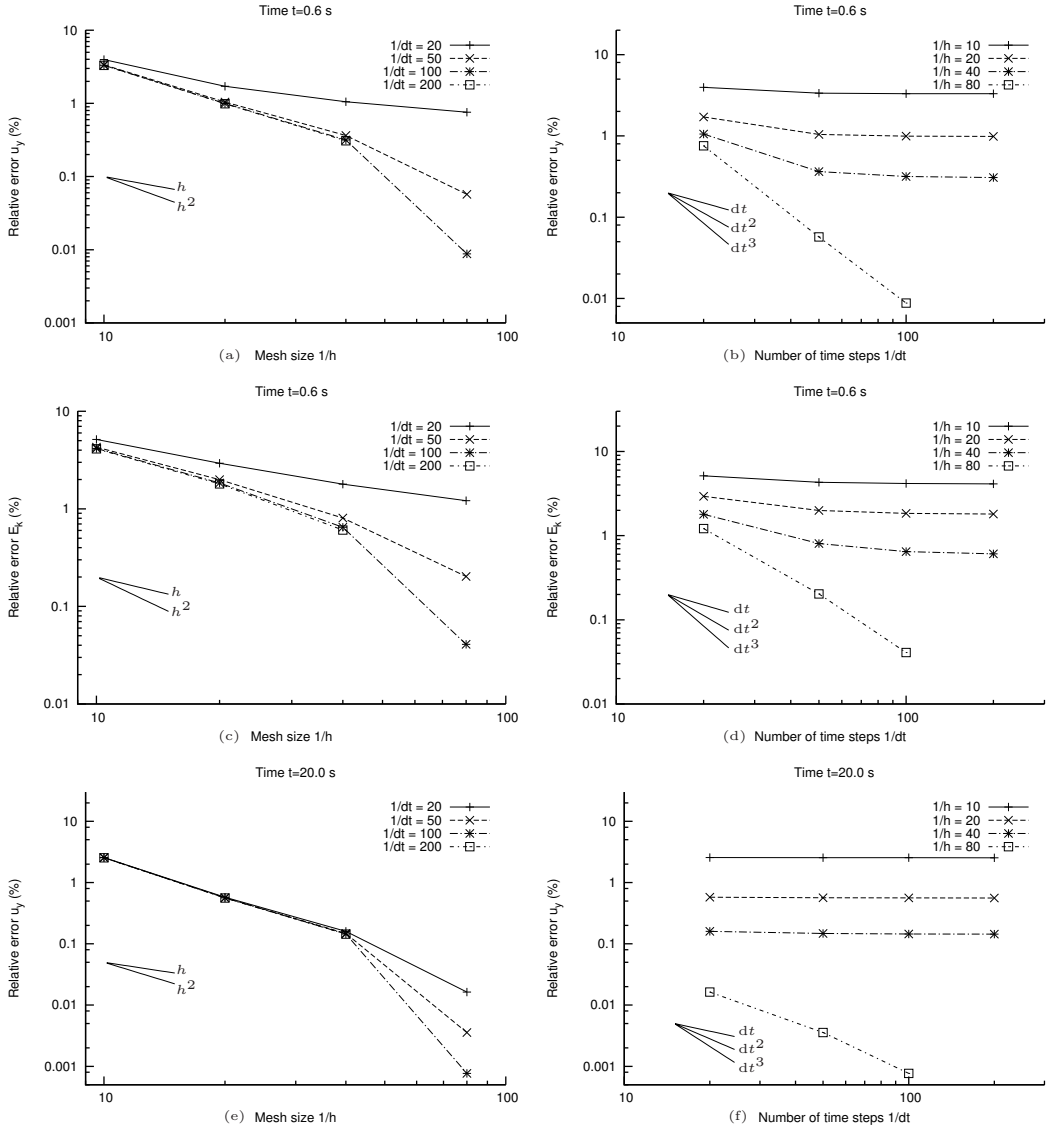

Figure 6: (a), (b): Graphs for the dependence of the relative error of deformation u_y on the mesh size h and the time step Δt at $t = 0.6$ s, (c), (d): relative error for E_k for the mesh size h and time step Δt at $t = 0.6$ s, (e), (f):relative error for u_y for the mesh size h and the time step Δt at $t = 20$ s.

mesh\timestep	0.05	0.02	0.01	0.005
mesh1	97.6757	96.8109	96.6711	96.6358
mesh2	95.4497	94.5366	94.3909	94.3542
mesh3	94.3437	93.4059	93.2570	93.2195
mesh4	93.7926	92.8423	92.6919	92.6540

Table 4: Kinetic energy E_k at $t = 0.6$ s for all four meshes and all four time steps with the Glowinski time scheme.

mesh\timestep	0.05	0.02	0.01	0.005
mesh1	-0.0452265	-0.0452183	-0.0452161	-0.0452156
mesh2	-0.0443225	-0.0443169	-0.0443155	-0.0443152
mesh3	-0.0441374	-0.0441317	-0.0441305	-0.0441301
mesh4	-0.0440739	-0.0440683	-0.0440671	-0.0440667

Table 5: Deformation u_y in the middle of the top side at $t = 20.0$ s for all four meshes and all four time steps with the Glowinski time scheme.

h^2 and for time of the order between Δt^2 and Δt^3, for the densest mesh. In the graphs a combination of discretization errors (space+time) is depicted. In the case of the coarse mesh the space discretization error is much higher than the time discretization error and so the relative error decreases very slowly with smaller time step and vice versa the relative error decreases slower with a smaller mesh size for a long time step.

Mesh stability. We compared the result obtained with mesh3 and time step $\Delta t = 0.01$ with the results obtained with the meshes where all inner nodes are randomly perturbed by 20% of h (mesh3d20) and 25% of h (mesh3d25, see Figure 7). The computational mesh is again

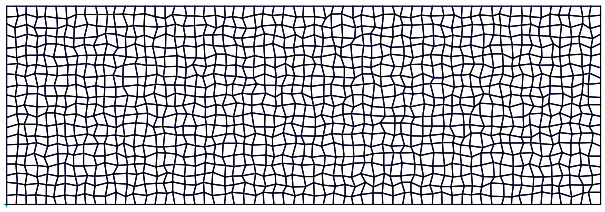

Figure 7: Mesh3d25 is mesh3 where all inner nodes are randomly perturbed by 25% of h.

the mesh locally refined near the boundary. In Table 6 one can see the deformation u_y at the center of the top surface and kinetic energy E_k at times $t = 0.6$ s and $t = 20$ s for these meshes. The change of relative error caused by the perturbed mesh is very small, approximately 200 times smaller than the relative error of u_y observed in the convergence analysis for mesh3 and $\Delta t = 0.01$ and approximately 20 times smaller than the relative error of E_k.

	u_y at $t = 0.6$	u_y at $t = 20$	E_k at $t = 0.6$
mesh3	-0.1052579	-0.04413047	93.2570
mesh3d20	-0.1052592	-0.04413016	93.2864
mesh3d25	-0.1052596	-0.04413021	93.2936

Table 6: Comparison of the results for perturbed meshes.

4.2. Problem 2 – Repeated loading and removal of load at specified locations

We next consider the problem wherein a specific portion of the body is repeatedly loaded and the load repeatedly removed. This problem has relevance to the problem of rutting that is observed on roadways due to the loading of the roadways by transportation vehicles. The tires of these vehicles constantly go over a small part of the roadway and one can clearly observe the depression that is made on the roadway. We are primarily interested in how the viscoelastic fluid responds and not in the specific problem of rutting. While there have been several attempts at modeling rutting in the asphalt mechanics literature, none of them are based on a rigorous thermodynamic basis for the model, nor do the numerical studies meet the criterior of convergence, stability, etc., that are usually found in numerically studies such as the one carried over here.

We assume that the roadway is made of an Oldroyd-B and the generalized Burgers' material defined through equation (16), the material parameters taking the values given in Table 1. Let us consider a rectangular piece of material as given in Figure 8. The width is 3m, the height is 0.5m. The loads are assumed to move along the z-direction as shown. We have assumed that the tires are 0.25m wide. At the bottom surface we will assume that the material can fully slip in the x-direction, but it can not move in the y-direction. The material can not flow through the lateral sides but it can fully slip in the y-direction. It can freely move on the top.

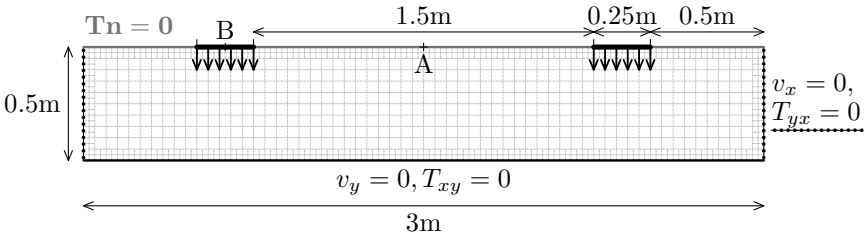

Figure 8: Problem 2.

The material is pushed by a constant normal stress $T_{yy} = -2$ kPa due to the contact of the tires on the body as depicted in Figure 8. Let us assume that there are fifteen passes over a particular region by the load that stays in contact with the body at that location for 0.5s, that is the region on the top surface on which compressive loads are displayed in Figure 8 is compressed fifteen times and the duration of the contact is 0.5s. Let us also assume the time interval between loads being applied at the same location is 3.5s. Thus, the body is

given 3.5s to relax. Let us suppose that the material is pressed between the times t_1^k and t_2^k, where $t_1^k = (4.0k)$ s and $t_2^k = (0.5 + 4.0k)$ s for $k = 0, \ldots, 14$.

The boundary conditions are:

Bottom surface Dirichlet: $v_y = 0$, Neumann: $T_{xy} = 0$

Lateral sides Dirichlet: $v_x = 0$, Neumann: $T_{yx} = 0$

Bottom corners Dirichlet: $v_x = v_y = 0$

Top surface Neumann: $\mathbf{Tn} = \mathbf{0}$, during the pressing $T_{yy} = -2$ kPa on a part of the boundary.

The time dependence of the deformation u_y of two points A and B on the top surface (see Figure 8) is depicted in Figure 9.

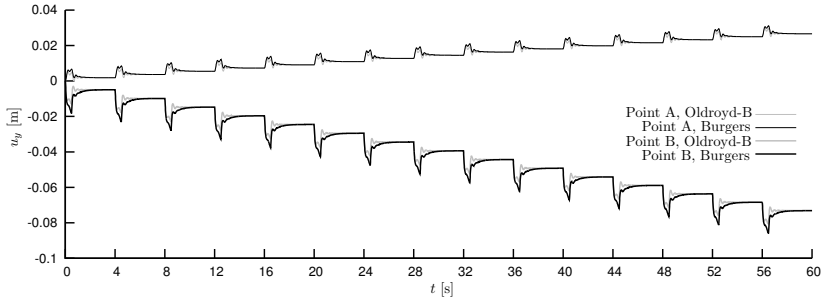

Figure 9: The time dependence of the deformation u_y at the points A (upper line) and B (lower line). The grey line corresponds to the generalized Burgers' model and the black line corresponds to the Oldroyd-B model.

In Figure 10 we depict the result of compressing the body comprised of a generalized Burgers fluid fifteen times as discussed. For the purpose of illustration, only the evolution of the deformation with time for their first, the eighth and the fifteenth compression is portrayed. Each compression is drawn in a different color. The beginning of the compression is denoted by a dotted line and the end by a dashed line and the deformation four seconds after the beginning of the compression by a solid line. The full movie of the problem can be seen at `http://artax.karlin.mff.cuni.cz/~tumak3am/Flow_of_a_Burgers_fluid/`.

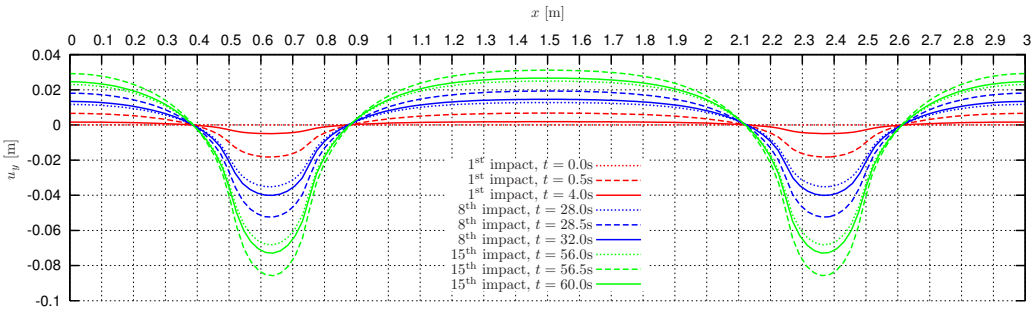

Figure 10: Time snapshots of the top side depicting the first (red line), the eighth (blue line) and the fifteenth (green line) application of force. Corresponding to these applications of compressive loads at the top surface the beginning of the application by a dotted line, the end of the application by a dashed line and the deformation four seconds after the beginning of the application by a solid line.

4.3. Problem 3 – Rolling over a viscoelastic material

The last problem is the rolling of a load on a rectangular viscoelastic body.

Let us consider the rectangular piece of material, the width is 3m, the height is 0.5m. The generalized Burgers' model is used (see Table 1). The problem is depicted in the Figure 11. The material is on the ground where it can fully slip in the x-direction, but it can not move in the y-direction. All other sides of the rectangle can freely move.

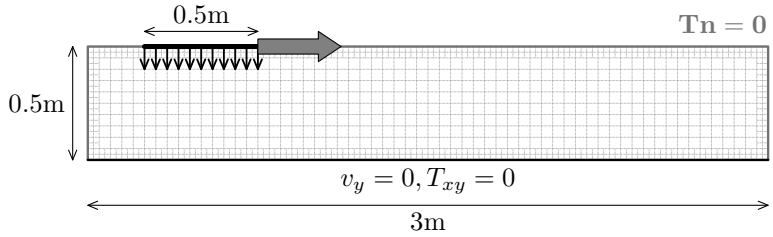

Figure 11: Problem 4.

At the beginning the material is at rest and does not move. Suddenly at time $t = 0$ it is pushed at the top with a constant normal stress $T_{yy} = -5$ kPa. The force is applied on the constant area $l = 50$cm, this area moves with the velocity 40 cm/s from the left to the right and then back to the left, i.e. the material is rolled forward and backwards. In the Figure 12 the location of the area and its boundaries is depicted with respect to time t. The load is released at $t = 10.4$ s and the material is let to relax.

The boundary conditions are:

Bottom surface Dirichlet: $v_y = 0$, Neumann: $T_{xy} = 0$

Top and sides Neumann: $\mathbf{Tn} = \mathbf{0}$, during the pressing $T_{yy} = -5$ kPa on the moving part of the boundary.

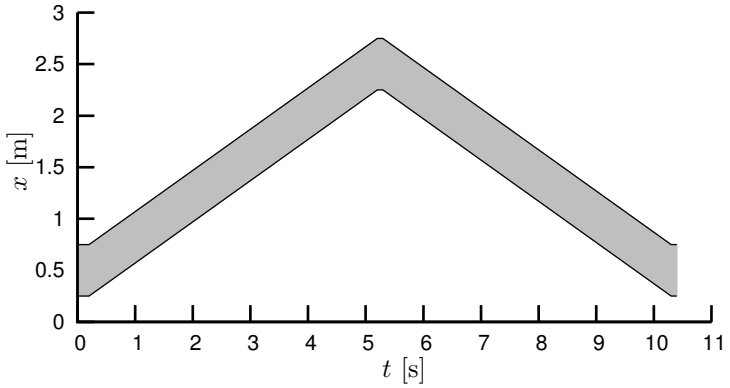

Figure 12: The location of the area where the force is applied with respect to time.

In the Figure 13 there are five snapshots of the whole simulation. It can be seen how the material is rolled into the sides, the snapshot at $t = 6.5$ s shows how the roller pushes the material ahead. The last two snapshots show the relaxation of the material due to the elastic part of response. The full movie of rolling is available at `http://artax.karlin.mff.cuni.cz/~tumak3am/Flow_of_a_Burgers_fluid/`.

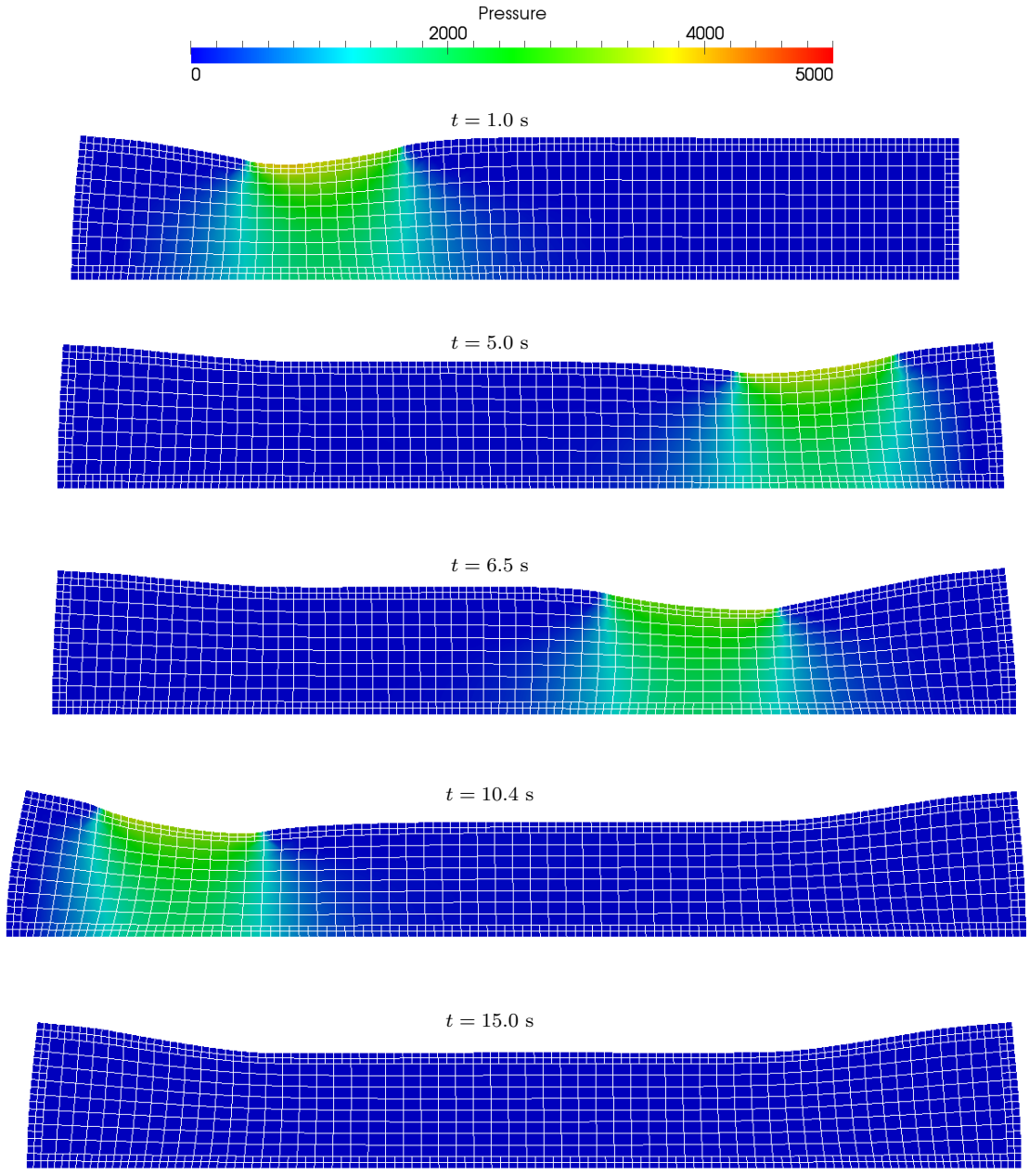

Figure 13: Snapshots of the rolling over a viscoelastic material.

Acknowledgements

J. Hron thanks the project GACR 107/12/0121 for its support. K.R. Rajagopal thanks the National Science Foundation for its support. K. Tůma was supported by the project GACR 201/09/0917 and the project LL1202 in the programme ERC-CZ funded by the Ministry of Education, Youth and Sports of the Czech Republic.

References

[1] J. C. Maxwell, On the dynamical theory of gases, Philos. Trans. R. Soc. 157 (1867) 49–88.

[2] J. M. Burgers, Mechanical considerations – model systems – phenomenological theories of relaxation and viscosity, in: First report on viscosity and plasticity, Nordemann Publishing, New York, 1939, pp. 5–67.

[3] J. G. Oldroyd, On the Formulation of Rheological Equations of State, Proc. Roy. Soc. London Ser. A 200 (1950) 523 – 541.

[4] H. Damanik, FEM Simulation of Non-isothermal Viscoelastic Fluids, Ph.D. Thesis, Technischen Universität Dortmund, 2011.

[5] S. A. White, A. D. Gotsis, D. G. Baird, Review of the entry flow problem: experimental and numerical, Journal of Non-Newtonian Fluid Mechanics 24 (1987) 121–160.

[6] R. Fattal, R. Kupferman, Constitutive laws for the matrix-logarithm of the conformation tensor, Journal of Non-Newtonian Fluid Mechanics 123 (2004) 281–285.

[7] M. A. Hulsen, R. Fattal, R. Kupferman, Flow of viscoelastic fluids past a cylinder at high weissenberg number: stabilized simulations using matrix logarithms, Journal of Non-Newtonian Fluid Mechanics 127 (2005) 27–39.

[8] A. Afonso, P. J. Oliveira, F. T. Pinho, M. A. Alves, The log-conformation tensor approach in the finite-volume method framework, Journal of Non-Newtonian Fluid Mechanics 157 (2009) 55–65.

[9] Y. Fan, H. Yang, R. I. Tanner, Stress boundary layers in the viscoelastic flow past a cylinder in a channel: limiting solutions, Acta Mechanica Sinica 21 (2005) 311–321.

[10] H. Damanik, J. Hron, A. Ouazzi, S. Turek, A monolithic FEM approach for the log-conformation reformulation (LCR) of viscoelastic flow problems, Journal of Non-Newtonian Fluid Mechanics 165 (2010) 1105–1113.

[11] J. Étienne, E. J. Hinch, J. Li, A Lagrangian–Eulerian approach for the numerical simulation of free-surface flow of a viscoelastic material, Journal of Non-Newtonian Fluid Mechanics 136 (2006) 157–166.

[12] H. Damanik, A. Ouazzi, S. Turek, Numerical simulation of a rising bubble in viscoelastic fluids, in: A. Cangiani, R. L. Davidchack, E. Georgoulis, A. N. Gorban, J. Levesley, M. V. Tretyakov (Eds.), Numerical Mathematics and Advanced Applications 2011, Springer Berlin Heidelberg, 2013, pp. 489–497.

[13] J. M. Krishnan, K. R. Rajagopal, Review of the uses and modeling of bitumen from ancient to modern times, Applied Mechanics Reviews 56 (2003) 149 – 214.

[14] M. J. Crochet, A. R. Davies, K. Walters, Numerical simulation of Non-Newtonian flow, Elsevier Science, 1984.

[15] K. R. Rajagopal, A. R. Srinivasa, A thermodynamic frame work for rate type fluid models, Journal of Non-Newtonian Fluid Mechanics 88 (2000) 207 – 227.

[16] S. Boyaval, T. Lelièvre, C. Mangoubi, Free-energy-dissipative schemes for the Oldroyd-B model, ESAIM: Mathematical Modelling and Numerical Analysis 43 (2009) 523–561.

[17] G. Scovazzi, T. Hughes, Lecture notes on continuum mechanics on arbitrary moving domains, Technical Report, Technical report SAND-2007-6312P, Sandia National Laboratories, 2007.

[18] R. Glowinski, Numerical methods for fluids (part 3). Finite element methods for incompressible viscous flow. Vol. 9 of Handbook of numerical analysis, P.G. Ciarlet and J.L. Lions, eds, 2003.

[19] S. Turek, L. Rivkind, J. Hron, R. Glowinski, Numerical study of a modified time-stepping θ-scheme for incompressible flow simulations, Journal of Scientific Computing 28 (2006) 533–547.

[20] T. A. Davis, Algorithm 832: Umfpack v4.3 – an unsymmetric-pattern multifrontal method, ACM Transactions on Mathematical Software (TOMS) 30 (2004) 196–199.

[21] R. B. Bramley, Splib software package, Indiana University, Bloomington, IN (1995).

[22] J. Hron, Fluid structure interaction with applications in biomechanics, Ph.D. Thesis, Charles University, 2001.